Noise–induced stabilization of bumps in systems with long–range spatial coupling

Carlo R. Laing [a,*] and André Longtin [a]

[a] *Department of Physics, University of Ottawa, 150 Louis Pasteur, Ottawa ON, Canada K1N 6N5.*

Abstract

The position of a localized region of active neurons (a "bump") has been proposed to encode information for working memory, the head direction system, and feature selectivity in the visual system. Stationary bumps are ordinarily stable, but including spike frequency adaptation in the neural dynamics causes a stationary bump to become unstable to a moving bump through a supercritical pitchfork bifurcation in bump speed. Adding spatiotemporal noise to the network supporting the bump can cause the average speed of the bump to decrease to almost zero, reversing the effect of the adaptation and "restabilizing" the bump. This restabilizing occurs for noise levels lower than those required to break up the bump. The restabilizing can be understood by examining the effects of noise on the normal form of the pitchfork bifurcation where the variable involved in the bifurcation is bump speed. This noisy normal form can be further simplified to a persistent random walk in which the probability of changing direction is related to the noise level through an Arrhenius–type rate. The probability density function of position for the continuous–time version of this random walk satisfies the telegrapher's equation, and the closed–form solution of this PDE allows us to find expressions for the mean and variance of the average speed of the particle (the bump) undergoing the random walk. This noise–induced stabilization is a novel example in which moderate amounts of noise have a beneficial effect on a system, specifically, stabilizing a spatiotemporal pattern.

Key words: Pattern formation, noise, bifurcation, integral coupling, neuroscience.
PACS: 47.54.+r, 05.40.-a, 02.30.Oz

* Corresponding author. ph: (613) 562 5800 extn. 6744, fax: (613) 562 5190.
Email addresses: claing@science.uottawa.ca (Carlo R. Laing), alongtin@physics.uottawa.ca (André Longtin).

1 Introduction

There has been much recent interest in spatially localized patches of active neurons ("bumps") as models for feature selectivity in the visual system [3,4,14], the head direction system [38], and working memory [5,12,22,44]. Both rate models [2,3,6,14,38], in which the firing rates of cells are the variables of interest, and networks of spiking neurons [4,5,12,22,39], in which the cells communicate by firing voltage "spikes", have been used in the study of such structures.

Spike frequency adaptation, in which the discharge frequency of a neuron slowly decreases under a constant stimulus, is ubiquitous in cortical neurons [26]. One previous study of rate and spiking models capable of bump formation, [14], noted that the inclusion of adaptation caused previously neutrally stable stationary bumps to become unstable, with bumps that travel at a constant speed being stable instead. This presumably has a deleterious effect on the systems mentioned above which are thought to be capable of sustaining stationary bumps. The main purpose of our work is to show that the addition of noise to such a system can counteract the destabilizing influence of adaptation. This "restabilizing" occurs in both spiking and rate models, and is an example, similar in spirit to stochastic resonance [9,45] and noise–enhanced propagation [17,27], of a situation in which moderate amounts of noise are necessary for a system to behave in an optimal fashion. In the neural context of interest here, noise is associated with random synaptic firing, as well as conductance fluctuations, both common in real neural systems [29].

To analyze the effect of the noise, we study a spatially–extended rate model that can be reduced to a set of six ordinary differential equations, and then show that this system of ODEs undergoes a supercritical pitchfork bifurcation [11] in bump velocity as the strength of the adaptation is increased — this is the source of the destabilization of a stationary bump as a result of including adaptation. We add noise to the normal form of the associated supercritical pitchfork bifurcation, where the variable undergoing the bifurcation is velocity, and investigate the effect of this noise on the total distance traveled (the time integral of the velocity) after the bifurcation has occurred, i.e. when the noise–free normal form has two stable non–zero velocity values of opposite sign. We see that for low noise values the distance traveled is proportional to time, but for larger noise values the instantaneous velocity will change signs, leading to some cancellation in the integral, and resulting in a smaller net distance traveled, as is observed in simulations of the spatially–extended networks.

We show that this switching in the noisy pitchfork bifurcation, where the velocity is a continuous variable, can be further simplified to a persistent random walk [32] in which a particle moves at a constant speed to either the right or the left on a line, and the probability of *changing* direction is constant (and related to the noise level through an Arrhenius–type rate). Both discrete and continuous–time versions of this random walk are discussed. In the continuous–time version, the position of the

particle is the time integral of Markovian dichotomous noise [16,41]. The probability density function satisfies the telegrapher's equation [15,32,41], which has an explicit solution, enabling us to find expressions for the mean and variance of the average distance moved during a fixed time for different noise levels.

The analysis of these random walks provides a good explanation for, and qualitative agreement with, the behavior seen in the full spiking neuron model. Furthermore, our analysis provides a novel example in which moderate amounts of noise have a beneficial effect on a system, since for the models mentioned above, moving bumps are undesirable.

While we have considered only neural systems, other model and experimental systems show spatially localized "spots" which can be made to travel at arbitrarily low speeds by changing a parameter [18,21,34,35,40], and similar restabilization by noise may be possible in these systems.

In Section 2 we show that adaptation in a network of spiking neurons destabilizes a stationary bump, as has been observed before [14], but Gaussian white noise restabilizes it. In Section 3 we show the same phenomenon in a rate model, and show that colored noise is even more effective than Gaussian white noise at stabilizing a bump. In Section 4 we convert the rate model studied in the previous section to a set of six ODEs, and show that the bump velocity undergoes a pitchfork bifurcation as adaptation strength is increased. Section 5 discusses the persistent random walk as a model for bump motion and Section 6 provides a summary. Appendix A has a derivation of the solution of the telegrapher's equation.

A short summary of much of the work discussed here has been presented elsewhere [23].

2 Spiking Model

In this section we demonstrate the phenomenon of noise–induced stabilization of "bumps" in a one–dimensional network of N integrate–and–fire neurons [4,22] with adaptation. The coupling extends beyond nearest–neighbor and involves local excitation and longer–range inhibition. The domain is a circle. (Similar networks have been used to model head direction [38] and feature selectivity in the visual system [3,4,14], and such a domain is natural in these models.) The equations governing the voltages, V_i, and adaptation currents, a_i, are

$$\frac{dV_i}{dt} = I_i - a_i - V_i + \frac{1}{N}\sum_{j,m} J_{ij}\alpha(t - t_j^m) - \sum_l \delta(t - t_i^l) \tag{1}$$

$$\tau_a \frac{da_i}{dt} = A\sum_l \delta(t - t_i^l) - a_i \tag{2}$$

for $i = 1, \ldots, N$, where the subscript i indexes the neurons, t_j^m is the mth firing time of neuron j, defined to be the times at which V_j crosses 1 from below, and $\delta(\cdot)$ is the Dirac delta, used to reset the voltage to zero and increment a. The function $\alpha(t)$ is a post–synaptic current, which we take to be $\beta e^{-\beta t}$ for $t \geq 0$ and zero otherwise; I_i is the constant current applied to neuron i. The connection strength between neuron i and neuron j is J_{ij}. The sums over m and l extend over the entire firing history of the neurons in the network and the sum over j extends over the whole network. The variable a_i is incremented by an amount A/τ_a whenever V_i reaches 1 from below, and decays exponentially with time constant τ_a otherwise.

For $A = 0$, the system (1) is known to support "bumps", spatially localized patches of active neurons [22]. Since the network is invariant with respect to spatial translation, there is actually a continuum of bumps, parametrized by their spatial location [14,22]. For small A, this behavior persists, but as A is increased further, a stationary bump loses stability to a traveling bump that can travel either leftwards or rightwards. Figure B.1 shows the absolute value of the speed of a bump as a function of A (adaptation strength), and an example of a traveling bump is shown in Figure B.2, left. Parameters for Figures B.1, B.2 and B.3 are $I_i = 0.95$, $N = 60$, $\tau_a = 5$, $\beta = 0.5$ and

$$J_{ij} = 5.4\sqrt{\frac{28}{\pi}} \exp\left[-28\left(\frac{i-j}{N}\right)^2\right] - 5\sqrt{\frac{20}{\pi}} \exp\left[-20\left(\frac{i-j}{N}\right)^2\right] \tag{3}$$

i.e. neurons excite nearby neighbors but inhibit distant ones. This form of coupling is sometimes referred to as "Mexican–hat" [6], and is prevalent in many parts of the nervous system. Note that J_{ij} depends only on the difference $|i - j|$.

The reason that adaptation causes a bump to move is as follows: adaptation can be thought of as a slow, activity–dependent subtractive current. Once a bump is moving, this subtractive current will be greater in magnitude at the trailing edge of the bump than at the leading edge, as the neurons at the trailing edge have been firing for longer. Since bumps are "attracted" to injections of positive current [6,14] (and "repelled" by negative current), the adaptation current will cause the bump to continue moving. A small asymmetry in initial conditions is sufficient to start the bump moving.

We add noise to the system by adding/subtracting (with equal probability, so the mean current is unchanged) current pulses of the form $\sigma e^{-t/\tau_I}$ $(t > 0)$ to/from each I_i. The arrival times of these pulses are chosen from a Poisson distribution with mean rate 0.075 Hz, and there is no correlation between arrival times for different neurons (i.e. the noise is zero–mean shot noise [36]). τ_I has the value 0.4. Adding noise in this form can significantly decrease the effective speed of the bump. An example is shown in Figure B.2 (right panel). Here, the speed is no longer constant, but we can easily measure the average speed during a simulation of fixed duration — it is the ratio of the distance moved by the center of the bump during the simulation to the duration of the simulation. Note that increasing the noise intensity far enough will break up the bump (not shown), as the noise will then dominate the coupling that keeps the bump together. Thus, stabilization occurs before break–up as noise intensity is increased.

The absolute value of this average speed during simulations of fixed duration as a function of noise level, σ, is shown in Figure B.3. The standard deviation of the absolute value of the average speed is also shown. For this Figure, and other similar ones, the absolute value of the average speed is $\langle |x(t)| \rangle / t$, where $x(t)$ is the distance traveled during time t and the angled brackets indicate averages over realizations, and the standard deviation of this quantity is calculated using $\sqrt{\langle |x(t)|^2 \rangle - \langle |x(t)| \rangle^2}/t$. We see that there are two regimes, with a rapid transition between them. For low noise, $\sigma < 0.03$, the bump travels at a constant, large velocity, to either the right or the left, but without switches in direction, an example being Figure B.2, left. For strong noise, $0.1 < \sigma$, the bump's average speed is low, as the noise seems to disrupt the mechanism (adaptation) that is responsible for the destabilization of the stationary bump. An example is Figure B.2, right. In the transition regime, $0.03 < \sigma < 0.1$, the bump travels at a nearly constant speed, but makes one or more abrupt switches in direction during the simulation (not shown), leading to a smaller average velocity. It is this effective "slowing down" of the bump (in the sense that the average speed during a fixed amount of time is reduced, rather than the instantaneous speed) that we are concerned with in this paper.

The fact that noise stabilizes a bump before breaking it up in the system (1)-(2) is in contrast with the behavior seen in e.g. a network of diffusively coupled Fitzhugh–Nagumo excitable elements:

$$\frac{du_i}{dt} = u_i - u_i^3/3 - v_i + D\left(\frac{u_{i+1} - 2u_i + u_{i-1}}{(\delta x)^2}\right) \tag{4}$$

$$\frac{dv_i}{dt} = \epsilon(u_i - \gamma v_i + b) + \xi(t) \tag{5}$$

where $\xi(t)$ is a Gaussian white noise term with $\langle \xi(t) \rangle = 0$ and $\langle \xi(t)\xi(s) = 2\sigma\delta(t-s)$. A traveling wave for this network is shown in Figure B.4, and noise with two different intensities is added after some time. Small noise intensities (Figure B.4, left) cause fluctuations in the wave's profile but do not significantly affect its speed, whereas larger intensities (Figure B.4, right) cause the wave to break up rather than slow down.

3 Rate Model

In this section we study a rate model that includes adaptation. Rate models differ from spiking models in that the quantity of interest is the rate of spiking. Using this description of a network often allows the use of analytical methods [6]. The rate model we use is

$$\frac{\partial u(x,t)}{\partial t} = -u(x,t) + \int_\Omega J(x-y)F[I(y,t) + u(y,t) - a(y,t)]\,dy \tag{6}$$

$$\tau_a \frac{\partial a(x,t)}{\partial t} = Au(x,t) - a(x,t) \tag{7}$$

Here, we have let $N \to \infty$, so that space (x) is a continuous variable; Ω is the domain. $u(x,t)$ is the synaptic input to neurons at position x, and $a(x,t)$ is the adaptation current at position x. $F[w]$ is a transfer function that converts the current flowing into a neuron, w, to the activity of that neuron. Equation (6), with $a = 0$, has been discussed by a number of authors [2,6,22] with respect to the formation of stationary patterns of activity (bumps). Laing and Chow [22] showed that an equation of the form (6) could be derived from a network of integrate–and–fire neurons under the assumptions that the post–synaptic current, $\alpha(t)$, was a Dirac delta function, and that the neurons were firing asynchronously. The function $F[\cdot]$ was the "f-I curve", or the function giving the frequency of firing for a constant input current, I, for an isolated integrate–and–fire neuron.

Adaptation was included in (1)-(2) as a subtractive current, and we keep that form in (6)-(7). We want $a(x,t)$ to increase when the neurons at x are active and decay back to zero otherwise, on a time–scale given by τ_a. Thus it would be more appropriate to use $F[I + u(x,t) - a(x,t)]$ instead of $u(x,t)$ as the "drive" for a in (7). However, our choice of using $u(x,t)$ considerably simplifies the later analysis, and the effect that we are investigating (stabilization by noise of bumps that have been destabilized by adaptation) is observed in (6)-(7), as well as in these equations with $u(x,t)$ in (7) replaced by $F[I + u(x,t) - a(x,t)]$ (not shown).

Equations (6)-(7) are similar to those studied in Ref. [14]. These authors also saw destabilization of a stationary bump to a moving bump as the strength of adaptation was increased, and the velocity of the moving bump increased monotonically with adaptation strength.

In a similar way to the system (1)-(2), (6)-(7) also supports stationary bumps when A is small, which become unstable to traveling bumps as A is increased. (See Figure B.8 for a plot of speed versus A.) The parameter values used are $I = -0.1$, $A = 0.2$ and $\tau_a = 5$, with $J(x) = 0.05 + 0.24\cos x$ and $F[u] = 0.5[1 + \tanh(10u)]$. The domain, Ω, is the line, $[0, 2\pi)$, with periodic boundary conditions. The system is integrated by spatially discretizing it to 100 points, giving a system of 200 coupled ODEs. Explicitly, they are

$$\frac{du_i}{dt} = -u_i + \frac{2\pi}{100}\sum_{j=1}^{100} J_{ij}F[I_j + u_j - a_j] \tag{8}$$

$$\tau_a \frac{da_i}{dt} = Au_i - a_i \tag{9}$$

for $i = 1, \ldots, 100$, where $J_{ij} = J(2\pi|i-j|/100)$ and $I_j = -0.1$ for all j.

3.1 Gaussian white noise

First we consider adding independent Gaussian white noise terms, $\xi_i(t)$, to each of the differential equations for the a_is, i.e. we replace (9) with

$$\tau_a \frac{da_i}{dt} = Au_i - a_i + \xi_i(t) \tag{10}$$

where $\langle \xi_i(t) \rangle = 0$, $\langle \xi_i(t)\xi_j(s) \rangle = 2D\nu_{ij}\delta(t-s)$, and $\nu_{ij} = 0$ if $i \neq j$, and 1 if $i = j$. As with the spiking model, the average speed of these traveling bumps can be markedly reduced by adding noise to the system, as shown in Figure B.5, even though in this case the noise has a continuous state space, rather than being shot noise as in the spiking neuron model of Section 2.

Figure B.5 is qualitatively similar to Figure B.3, but there is a difference with regard to the variability of bump speed at low noise levels. For low noise levels a traveling bump in the rate model has a well–defined velocity, but in the full spiking model a traveling bump is the result of the collective behavior of a number of units, each of which has its own spiking dynamics. Even if no noise is added to the system, these dynamics contribute to fluctuations in any quantity associated with the network as a whole, and lead to the relatively large fluctuations in the speed of the bump at low noise levels in Figure B.3. These fluctuations do not appear in Figure B.5 because the rate model is derived from a network with an infinite number of asynchronous neurons whose fluctuations average out. The deterministic fluctuations in bump size and shape seen in Figure B.2, left, may actually act in the same way as the noise does in Figure B.2, right, stabilizing the bump to some extent, although obviously not to the same extent as the external noise.

3.2 Colored Noise

In this section we investigate the effect of temporal correlations in the noise process. We do this by adding independent colored noise terms, $\eta_i(t)$, to each of the differential equations for the a_i's, i.e. we replace (9) with

$$\tau_a \frac{da_i}{dt} = Au_i - a_i + \eta_i(t) \tag{11}$$

where $\langle \eta_i(t) \rangle = 0$, $\{\langle \eta_i(t)\eta_j(s) \rangle\} = \varepsilon\nu_{ij}e^{-|t-s|/\tau}$, ν_{ij} is as in Section 3.1, and $\{\cdots\}$ indicates averaging over the initial distribution of $\eta(0)$ values, taken from a Gaussian with mean zero and variance ε [7]. This type of noise, known as Ornstein–Uhlenbeck noise, also has a continuous state space.

Figure B.6, top, shows a plot of the absolute value of the average speed as a function of noise power, ε, for different correlation times, τ, as well as for frozen (i.e. time

independent) noise taken from the same distribution from which the $\eta(0)$ values are chosen. Figure B.6, bottom, shows the standard deviation of the absolute value of the average speed, plotted separately for clarity. Note the rise and then fall of the standard deviation as noise strength is increased — this behavior is explained qualitatively in Section 5.2. The qualitative behavior (slowing down of the bump) does not depend on the noise correlation time, but it is clear that when the noise level is high enough to significantly slow the bump, a larger value of τ leads to a smaller average velocity. This can be understood in terms of the limiting case, frozen noise, where the noise can "pin" the bump so that it has zero velocity for all time, with the spatial disorder overcoming the adaptation–induced tendency to move. (See [14,22] for examples of the pinning of a bump with spatial disorder in networks of spiking neurons. A similar phenomenon is the failure of a calcium wave to propagate due to inhomogeneities [43].) When the noise is correlated over a significant amount of time, τ, it is possible for the bump to be pinned for an amount of time comparable to this before moving again when the noise has significantly changed. These "pinning episodes" contribute to the lower average velocity. Thus, externally imposed (and slowly varying) disorder may be more effective in slowing the bump than fast intrinsic noise.

This behavior is further illustrated in Figure B.7, where we show the absolute value of the average speed (top) and average of the absolute value of the instantaneous speed (bottom) as functions of correlation time, τ, for a noise intensity sufficient to significantly slow the bump. It is clear that for both measures of speed, bump speed decreases as the noise correlation time increases. The absolute value of the average speed is a measure of how far the bump is from its starting position after a fixed amount of time, and is perhaps the most relevant quantity in a model of working memory (where bump position encodes some feature of the memory), but measuring the average of the absolute value of the instantaneous speed gives a better indication of the fraction of time that a bump is "pinned" during a particular simulation.

Adding spatial correlations to the noise, as in e.g. [37], may change the effect of noise on the bump, but we do not investigate that here.

4 Reduction to ODEs

Having satisfied ourselves that the rate model in Section 3 behaves qualitatively the same as the full spiking model in Section 2, both with and without noise, we will now show that the bifurcation from stationary to traveling bumps in (6)-(7) is a pitchfork bifurcation [11]. By an appropriate choice of the function J in (6), we can reduce the system (6)-(7) to a set of six ordinary differential equations. Consider the system (6)-(7), where $\Omega = [0, 2\pi)$ with periodic boundary conditions and $J(v) = B + C\cos v$, so that $J(x-y) = B + C\cos x\cos y + C\sin x\sin y$. (If C is positive, this choice of J can be thought of as the first two terms in a Fourier series expansion of a "Mexican–hat" type J [3,14].) We can expand u and a as Fourier series in x, but by doing so

and then substituting into (6)-(7), one can see that coefficients of terms of the form $\cos(nx)$ and $\sin(nx)$ for $n > 1$ will decay exponentially to zero, so we do not include terms of this form in the expansion. We write $u(x,t) = \alpha(t) + R(t)\cos(x - \theta(t))$ and $a(x,t) = \gamma(t) + \kappa(t)\cos(x - \theta(t) - \psi(t))$, where R and κ are positive. u has a maximum at $x = \theta$, and a has a maximum at $x = \theta + \psi$, so ψ measures the "phase lag" between the maxima of u and a. Substituting these expressions for $u(x,t)$ and $a(x,t)$ into (6)-(7) we obtain

$$\begin{aligned}
&\frac{d\alpha}{dt} + \cos(x-\theta)\frac{dR}{dt} + R\sin(x-\theta)\frac{d\theta}{dt} = -[\alpha + R\cos(x-\theta)] \\
&+B\int_0^{2\pi} F[I + \alpha + R\cos(y-\theta) - \gamma - \kappa\cos(y-\theta-\psi)]\,dy \\
&+C\cos x\int_0^{2\pi} F[I + \alpha + R\cos(y-\theta) - \gamma - \kappa\cos(y-\theta-\psi)]\cos y\,dy \\
&+C\sin x\int_0^{2\pi} F[I + \alpha + R\cos(y-\theta) - \gamma - \kappa\cos(y-\theta-\psi)]\sin y\,dy
\end{aligned} \tag{12}$$

and

$$\begin{aligned}
&\tau\left[\frac{d\gamma}{dt} + \cos(x-\theta-\psi)\frac{d\kappa}{dt} + \kappa\sin(x-\theta-\psi)\left(\frac{d\theta}{dt} + \frac{d\psi}{dt}\right)\right] \\
&= A[\alpha + R\cos(x-\theta)] - [\gamma + \kappa\cos(x-\theta-\psi)]
\end{aligned} \tag{13}$$

Fourier transforming these equations we obtain the 6 ODEs:

$$\frac{d\alpha}{dt} = -\alpha + Bf(\alpha-\gamma, R, \kappa, \psi) \tag{14}$$

$$\frac{dR}{dt} = -R + C[g(\alpha-\gamma, R, \theta, \kappa, \psi)\cos\theta + h(\alpha-\gamma, R, \theta, \kappa, \psi)\sin\theta] \tag{15}$$

$$\frac{d\theta}{dt} = \frac{C}{R}[h(\alpha-\gamma, R, \theta, \kappa, \psi)\cos\theta - g(\alpha-\gamma, R, \theta, \kappa, \psi)\sin\theta] \tag{16}$$

$$\tau\frac{d\gamma}{dt} = A\alpha - \gamma \tag{17}$$

$$\tau\frac{d\kappa}{dt} = AR\cos\psi - \kappa \tag{18}$$

$$\frac{d\psi}{dt} = -\frac{AR\sin\psi}{\tau\kappa} - \frac{d\theta}{dt} \tag{19}$$

where

$$f(\alpha-\gamma, R, \kappa, \psi) = \int_0^{2\pi} F[I + \alpha - \gamma + R\cos y - \kappa\cos(y-\psi)]\,dy \tag{20}$$

$$g(\alpha-\gamma,R,\theta,\kappa,\psi)$$
$$=\int_0^{2\pi} F[I+\alpha-\gamma+R\cos(y-\theta)-\kappa\cos(y-\theta-\psi)]\cos y\,dy \tag{21}$$

$$h(\alpha-\gamma,R,\theta,\kappa,\psi)$$
$$=\int_0^{2\pi} F[I+\alpha-\gamma+R\cos(y-\theta)-\kappa\cos(y-\theta-\psi)]\sin y\,dy \tag{22}$$

Note that f, being proportional to the spatial average of the bump's activity, does not depend on θ, the position of the center of the bump. We assume that R and κ are never zero, as such a solution would not correspond to a bump. Apart from transients, equations (14)-(19) are equivalent to equations (6)-(7), and we now show that stationary and moving bumps are solutions of (14)-(19), and that the transition between them is through a supercritical pitchfork bifurcation.

4.1 Stationary bumps

Fixed points of (14)-(19) correspond to stationary (zero velocity) bumps. From (19), $\psi=0$ or π at a fixed point. $\psi=0$ corresponds to a stable bump and $\psi=\pi$ to an unstable one, which we ignore from now on. We also have $\kappa=AR$ (from (18)) and $\gamma=A\alpha$ (from (17)), i.e. the bump in a is centered at the same place as the center of the bump in u, and is smaller by a factor of A.

As expected from the translational invariance of (6)-(7), the value of θ at a fixed point of (14)-(19) is arbitrary. We can see this by writing $F[\cdot]$ as a Fourier series:

$$F[I+\alpha-\gamma+R\cos(y-\theta)-\kappa\cos(y-\theta-\psi)]$$
$$=a_0+\sum_{n=1}^{\infty}[a_n\cos(n(y-\theta))+b_n\sin(n(y-\theta))] \tag{23}$$

where $a_0,\ldots,b_1\ldots$ are constant. The integrals in (21) and (22) will pick out only the coefficients with subscript 1, so

$$g(\alpha-\gamma,R,\theta,\kappa,\psi)=\pi[a_1\cos\theta+b_1\sin\theta] \tag{24}$$

and

$$h(\alpha-\gamma,R,\theta,\kappa,\psi)=\pi[a_1\sin\theta-b_1\cos\theta] \tag{25}$$

Thus, the term $g(\alpha-\gamma,R,\theta,\kappa,\psi)\cos\theta+h(\alpha-\gamma,R,\theta,\kappa,\psi)\sin\theta$ in (15) is actually equal to πa_1, a constant, and the term $h(\alpha-\gamma,R,\theta,\kappa,\psi)\cos\theta-g(\alpha-\gamma,R,\theta,\kappa,\psi)\sin\theta$ in (16) is equal to $-\pi b_1$, also a constant. Note that these statements are true irrespective of whether θ is constant or a function of time. When $\psi=0$, $F[I+\alpha-\gamma+R\cos(y-\theta)-\kappa\cos(y-\theta-\psi)]$ is even about $y=\theta$, so $b_1,b_2,\ldots$ are all zero. In

particular, $b_1 = 0$, making the right hand side of (16) zero, as it must be for a fixed point. Thus (14)-(19) has a continuum of fixed points, parametrized by the position of the maximum of the bump.

4.2 Moving bumps

From simulations of the rate model (6)-(7), we expect a fixed point of (14)-(19) to become unstable as A is increased, and the system to have an attractor on which $\theta(t) = \omega t$ for some non–zero and constant ω, with all other variables constant. Since $\theta \in \mathbf{S}^1$, this attractor is actually a periodic orbit. Assuming that we are on the attractor, $d\theta/dt = \omega$ and (18) and (19) give us

$$\psi = -\tan^{-1}(\tau\omega) \tag{26}$$

so that ψ is nonzero if and only if ω is nonzero. Also, remembering that $-\pi/2 < \psi < \pi/2$ for a stable bump, we see that ψ and ω have opposite signs. This is in agreement with our intuition about the model, viz. that the activity in a lags behind the activity in u. Equations (17) and (18) give $\gamma = A\alpha$ and $\kappa = AR\cos\psi < AR$, so the peak height in a of a moving bump is less than that of a stationary one. Substituting these values for ψ, κ and γ into (14)-(15) we see that on the attractor, α and R must simultaneously solve

$$\alpha = Bf\left[(1-A)\alpha, R, AR\cos\{-\tan^{-1}(\tau\omega)\}, -\tan^{-1}(\tau\omega)\right] \tag{27}$$

and

$$\begin{aligned} R = C\Big\{&\cos(\omega t)g\left[(1-A)\alpha, R, \omega t, AR\cos\{-\tan^{-1}(\tau\omega)\}, -\tan^{-1}(\tau\omega)\right] \\ &+ \sin(\omega t)h\left[(1-A)\alpha, R, \omega t, AR\cos\{-\tan^{-1}(\tau\omega)\}, -\tan^{-1}(\tau\omega)\right]\Big\} \end{aligned} \tag{28}$$

where the value of t in (28) is irrelevant, since (as shown in section 4.1) the function on the right hand side is independent of t. Let $\alpha = \tilde{\alpha}(\omega, A)$ and $R = \tilde{R}(\omega, A)$ be the equations that define the roots of (27)-(28), and define $\tilde{\psi}(\omega, A) = -\tan^{-1}(\tau\omega)$, $\tilde{\kappa}(\omega, A) = A\tilde{R}(\omega, A)\cos[\tilde{\psi}(\omega, A)]$, and $\tilde{\gamma}(\omega, A) = A\tilde{\alpha}(\omega, A)$. Then we can write (16) as

$$\begin{aligned} &C\Big[\cos(\omega t)h\left((1-A)\tilde{\alpha}(\omega,A), \tilde{R}(\omega,A), \omega t, \tilde{\kappa}(\omega,A), \tilde{\psi}(\omega,A)\right) \\ &-\sin(\omega t)g\left((1-A)\tilde{\alpha}(\omega,A), \tilde{R}(\omega,A), \omega t, \tilde{\kappa}(\omega,A), \tilde{\psi}(\omega,A)\right)\Big] \\ &-\tilde{R}(\omega,A)\omega = 0 \end{aligned} \tag{29}$$

or

$$\omega G(\omega, A) = 0 \tag{30}$$

i.e. a scalar equation in one variable, parametrized by A. We write it in this form because we know that $\omega = 0$ is always a fixed point of (14)-(19), and, from section 4.1, there is no dependence on t in (29). ($\omega = 0$ is always a solution of (30) because if $\omega = 0$, $\psi = 0$, and therefore b_1 in the Fourier representation of $F[\cdot]$, (23), is zero, making the right hand side of (16) zero.) We also know that $\omega G(\omega, A)$ is an odd function of ω (therefore $G(\omega, A)$ is even in ω). To see this, note that $\widetilde{R}(-\omega, A) = \widetilde{R}(\omega, A)$, and it can be shown that $g(\alpha - \gamma, R, -\omega t, \kappa, -\psi) = g(\alpha - \gamma, R, \omega t, \kappa, \psi)$ and $h(\alpha - \gamma, R, -\omega t, \kappa, -\psi) = -h(\alpha - \gamma, R, \omega t, \kappa, \psi)$, so the left hand side of (29) is an odd function of ω.

We expect two nonzero solutions of (30), of equal magnitude but opposite sign, to be created as A increases through some critical value. To show that this occurs, we expand $G(\omega, A)$ as a Taylor series. We can expand about $\omega = 0$, but should not expand about $A = 0$, as this is a singular limit. Instead, we choose to expand about $A = 0.15$, i.e. we write

$$G(\omega, A) = \mu_1 + \mu_2(A - 0.15) + \mu_3\omega^2 + \mu_4(A - 0.15)^2 + \cdots \tag{31}$$

The value $A = 0.15$ was chosen arbitrarily — we expect the bifurcation to occur at a small positive value of A. The series expansion, (31), will be more accurate for values of A closer to the bifurcation value ($A \approx 0.165$, from Figure B.8) for a given truncation of the series, but as can be seen below, this value works well. Approximate values of the four coefficients $\mu_1, \ldots, \mu_4$ can be found by numerically differentiating (30), as explained in [25]. For the parameter values given in Section 3 we find $\mu_1 \approx -0.0438$, $\mu_2 \approx 2.6012$, $\mu_3 \approx -9.986$ and $\mu_4 \approx 1.762$. In Figure B.8 we have plotted with a solid line

$$\omega = \sqrt{\frac{-[\mu_1 + \mu_2(A - 0.15) + \mu_4(A - 0.15)^2]}{\mu_3}} \tag{32}$$

when the expression under the square root is positive, i.e. approximate nonzero roots of (30), together with measured values of ω for the system (6)-(7) and (14)-(19). The agreement is very good, even having truncated $G(\omega, A)$ after quadratic order.

Thus we have shown that the instability to traveling bumps as A is increased in the integro–differential system (6)-(7) is due to a pitchfork bifurcation in the speed of a bump. The pitchfork bifurcation is supercritical.

4.3 Noisy pitchfork bifurcation

We now consider the effect of adding noise to the normal form of a supercritical pitchfork bifurcation in which the variable is speed. Instead of examining the behavior of this variable, we look at its integral over a fixed amount of time. We can use this to derive a quantity equivalent to the absolute value of the average speed of a bump, as plotted in Figures B.3 and B.5. The intuition behind this procedure is that the velocity reverses sign at random times, and since the velocity undergoes a pitchfork

bifurcation, we make the ansatz that the main effect of noise on the whole system will also appear in the normal form of that bifurcation [19].

Consider the system

$$\begin{aligned} \dot{\omega} &= \omega(\lambda - \omega^2) + \xi(t) \\ \dot{\theta} &= \omega \end{aligned} \tag{33}$$

where θ represents the position of the maximum of the bump and λ plays the role of A above. ξ is a Gaussian white noise term with autocorrelation $\langle \xi(t)\xi(s) \rangle = 2D\delta(t-s)$. $\lambda < 0$ corresponds to the case A less than the bifurcation value (~ 0.165 in Figure B.8). In this case, $\omega = 0$ is a stable fixed point, and the average velocity is zero. For $\lambda > 0$ and $D = 0$, there are two stable values of ω, namely $\pm\sqrt{\lambda}$, corresponding to left and rightward–moving bumps. The absolute value of the velocity is then $\sqrt{\lambda}$ when $\lambda > 0$ and the absolute value of the distance moved after time t, i.e.

$$|\theta(t) - \theta(0)| = \left| \int_0^t \omega(s)\, ds \right| \tag{34}$$

is proportional to t. For $D > 0$ there is the possibility of $\omega(t)$ changing sign over time, which leads to some cancellation in the integral. This cancellation causes a the drop in the absolute value of the average speed during a simulation of duration T, $|\theta(T) - \theta(0)|/T$, as shown in Figure B.9.

Another way to understand the effect of noise is to examine the behavior of (33) as a function of λ for different noise levels — see Figure B.10. We see that for low noise levels the average speed is close to the deterministic expression, $\sqrt{\lambda}$ for $\lambda > 0$, zero otherwise. For larger noise levels there is an interval of λ values (approximately $0 < \lambda < 0.5$ in Figure B.10) for which the average speed is much less than its noise–free value. The size of this interval increases with increasing noise level. Thus noise can be thought of as "delaying" the bifurcation in the sense that it increases the value of λ beyond which the average speed of the bump is appreciably greater than zero. This delaying is also seen in a plot of bump speed versus A for (6)-(7) (not shown), and is an example of the postponement [16,28] of a pitchfork bifurcation. Note that this delay will not occur in (33) if we just examine the probability density function for ω, since noise–induced transitions are not possible in one dimension [16]. It may, however, occur in a dynamical equation for $|\omega|$, an issue under investigation.

The process of deriving normal forms for bifurcations in noisy systems is discussed in [19,42], and although we do not make a quantitative connection between the noise strength in the full system of (8), (10) and in the one–dimensional normal form (33), the qualitative behavior in the vicinity of the bifurcation should be the same for the two systems.

5 Persistent Random Walk

As a further simplification of the noisy supercritical pitchfork bifurcation normal form, we model the motion of a bump as a persistent random walk with constant velocity [32], where the probability of *changing* direction, rather than that of going in a certain direction, is fixed. The advantage of this form of model is that it allows us to gain even more analytical insight into the full dynamics of the stochastic model (8), (10) than was possible with the stochastic normal form, (33).

5.1 Discrete time

First, consider the walk on a lattice, i.e. a discrete time process with constant time–step. Let p be the probability of not changing direction (so the probability of changing direction is $1-p$), and consider a walk with three steps. We use "0" to indicate a step to the right and "1" a step to the left. The possible paths, the probabilities of taking these paths, and the total distance moved are shown in Table C.1, where the factor of $1/2$ comes from the initial choice of moving left or right.

The probabilities of going a distance x, $P(x)$, are then

$$P(3) = p^2/2 \tag{35}$$
$$P(1) = p(1-p) + (1-p)^2/2 \tag{36}$$
$$P(-1) = p(1-p) + (1-p)^2/2 \tag{37}$$
$$P(-3) = p^2/2 \tag{38}$$

and from $P(x)$ it is straightforward to calculate the mean and variance of the absolute value of distance traveled as a function of p.

It is possible to enumerate all possible paths of a given length and calculate $P(x)$, but the number of possible paths increases exponentially with path length. A more efficient method results from noting that it is possible to calculate $P(x)$ for $n+1$ steps in terms of $P(x)$ for n steps, i.e. to use recursion. Our presentation follows Masilover and Weiss [32]. It is necessary to keep track of the direction from which the walker arrived at its current position. (This is similar to the approach of Masoliver et al. [30,31] for calculating mean first passage times for non–Markovian processes.) Let $q_n(x)$ be the probability that the walker is at position x at time n, having been at $x-1$ at the previous time step, and $r_n(x)$ be the probability that the walker is at position x at time n, having been at $x+1$ at the previous time step. Then

$$q_{n+1}(x) = pq_n(x-1) + (1-p)r_n(x-1) \tag{39}$$

and

$$r_{n+1}(x) = pr_n(x+1) + (1-p)q_n(x+1) \tag{40}$$

$P(x)$ for a given n is the sum of $r_n(x)$ and $q_n(x)$. Note that if n is odd (even), the only possible values of x are odd (even). Using this notation, Table C.1 gives

$$q_3(3) = p^2/2 \tag{41}$$
$$q_3(1) = (1-p)^2/2 + p(1-p)/2 \tag{42}$$
$$q_3(-1) = p(1-p)/2 \tag{43}$$
$$r_3(1) = p(1-p)/2 \tag{44}$$
$$r_3(-1) = (1-p)^2/2 + p(1-p)/2 \tag{45}$$
$$r_3(-3) = p^2/2 \tag{46}$$

with all other probabilities being zero, and this provides the first step in the recurrence relationship. Note the special case $p = 1$, which gives $q_n(n) = 1/2$ and $r_n(-n) = 1/2$ for all n, with all other probabilities being zero, so that the expected value of $|x|$ is n, with variance zero. Examples of $P(x)$ at different times and for two different values of p are shown in Figure B.11. The top panel has $p = 0.95$, and the strong peaks corresponding to never changing direction are clear. The lower panel has $p = 0.7$, and the distribution is more Gaussian–like, although it must have finite support, as $q_n(k)$ and $r_n(k)$ must both be zero for $n < |k|$.

Figure B.12 shows the average speed of a particle undergoing a persistent random walk with speed 1 as a function of noise level. To relate the probability of continuing in the same direction, p, to the noise level, D, we use an Arrhenius–type rate associated with the rate of activation of a particle over a barrier [10]. Such a barrier crossing is likened here to the changes of direction of the bump — more specifically to the barrier crossing of ω in (33). (Note that (33) corresponds to the motion of a particle in a double well potential.) Specifically, we have $1 - p = e^{-1/D}$. The factor of 1 in the exponent is chosen for simplicity — in section 5.2 we fit such an Arrhenius–type rate to numerically–obtained data.

The peak in the dashed curve in Figure B.12 near $D = 0.2$ is misleading in that it suggests that it is possible for a particle to move faster than 1, which it clearly cannot. The reason for this peak is that the variance grows very quickly once the noise level is high enough ($0.1 < D$ in Figure B.12) so that bumps can make a small number of changes of direction during a walk. Note that the peak in Figure B.12 is also observed in the plot of the absolute value of the average speed of a bump in the rate model (Figure B.5), for the normal form of the pitchfork bifurcation with noise (Figure B.9), and could be seen in Figure B.6 if we had plotted mean $\pm$ standard deviation.

The continuous time version of a persistent random walk is the stochastic differential equation

$$\frac{dx}{dt} = I(t) \tag{47}$$

where $I(t) \in \{-v, v\}$ and the probability that $I(t)$ switches from $-v$ to v, or from v to $-v$, in time interval dt is $\frac{1}{2}\beta\, dt$. In other words, the velocity is just dichotomous Markovian noise. Then the probability density function of x, $p(x,t)$, is known [13,16,41] to satisfy the integro–differential equation

$$\frac{\partial p(x,t)}{\partial t} = v^2 \int_{-\infty}^{t} e^{-\beta(t-s)} \frac{\partial^2 p(x,s)}{\partial x^2}\, ds \tag{48}$$

Differentiating this with respect to time we obtain the telegrapher's equation [15,32,41]:

$$\frac{\partial^2 p}{\partial t^2} + \beta \frac{\partial p}{\partial t} = v^2 \frac{\partial^2 p}{\partial x^2} \tag{49}$$

(An alternative derivation of (49) as the continuous version of the persistent random walk discussed in Section 5.1 is given in [32].) The solution of (49) with initial conditions $p(x,0) = \delta(x)$ (i.e. the particle starts at the origin) and $\partial p(x,t)/\partial t|_{t=0} = 0$ is derived in Appendix A (see also [15]). It is

$$\begin{aligned} p(x,t) = \frac{e^{-\beta t/2}}{2} \Bigg\{ \delta(x-vt) + \delta(x+vt) + H\left(vt - |x|\right) \Bigg[\frac{\beta}{2v} I_0\left(\frac{\beta}{2v}\sqrt{v^2t^2 - x^2}\right) \\ + \frac{\beta t}{2\sqrt{v^2t^2 - x^2}} I_1\left(\frac{\beta}{2v}\sqrt{v^2t^2 - x^2}\right) \Bigg] \Bigg\} \end{aligned} \tag{50}$$

where $H(\cdot)$ is the Heaviside step function and I_n is the modified Bessel function of the first kind of order n. (Note that this equation is also given (although incorrectly) in both [32,41].) The delta functions describe the motion of particles that never change direction. The Heaviside function reflects the fact that no particle can travel at a speed greater than v, and the Bessel functions describe the motion of particles that change direction at least once. The $p(x,t)$ in (50) has the same form as the $P(x)$ in Section 5.1, except that the spatial and temporal domains are now continuous (not shown).

The mean of the absolute value of the distance traveled after time t is then

$$\langle |x(t)| \rangle = 2\int_0^\infty xp(x,t)\,dx = e^{-\beta t/2}\left\{ vt + \frac{\beta}{2v}\int_0^{vt} xI_0\left(\frac{\beta}{2v}\sqrt{v^2t^2-x^2}\right)dx \right.$$
$$\left. + \frac{\beta t}{2}\int_0^{vt} \frac{x}{\sqrt{v^2t^2-x^2}} I_1\left(\frac{\beta}{2v}\sqrt{v^2t^2-x^2}\right)dx \right\}$$
$$= vte^{-\beta t/2}\left\{ I_1\left(\frac{\beta t}{2}\right) + I_0\left(\frac{\beta t}{2}\right)\right\} \tag{51}$$

where the angled brackets represent averaging over realizations.

To obtain the second moment of $|x(t)|$ (or $x(t)$) we note that after taking the spatial Fourier transform of $p(x,t)$,

$$\sigma(s,t) \equiv \int_{-\infty}^{\infty} p(x,t)e^{-isx}\,dx \tag{52}$$

we have

$$\langle |x(t)|^2 \rangle = \langle x^2(t) \rangle = -\frac{\partial^2 \sigma(s,t)}{\partial s^2}\bigg|_{s=0} \tag{53}$$

As derived in Appendix A, eq. (A.5),

$$\sigma(s,t) = e^{-\beta t/2}\left(\frac{\beta}{2} + \frac{\partial}{\partial t}\right)\left\{ \frac{1}{\sqrt{v^2s^2 - \beta^2/4}} \sin\left(t\sqrt{v^2s^2-\beta^2/4}\right)\right\} \tag{54}$$

We find that

$$\frac{\partial^2}{\partial s^2}\left\{ \frac{1}{\sqrt{v^2s^2-\beta^2/4}} \sin\left(t\sqrt{v^2s^2-\beta^2/4}\right)\right\}\bigg|_{s=0}$$
$$= -4v^2[\beta t\cosh(\beta t/2) - 2\sinh(\beta t/2)]/\beta^3 \tag{55}$$

and substituting this into (53),(54) we have

$$\langle |x(t)|^2 \rangle = \frac{4v^2e^{-\beta t/2}}{\beta^3}\left(\frac{\beta}{2} + \frac{\partial}{\partial t}\right)\left[\beta t\cosh\left(\frac{\beta t}{2}\right) - 2\sinh\left(\frac{\beta t}{2}\right)\right] \tag{56}$$
$$= \frac{2v^2(\beta t - 1 + e^{-\beta t})}{\beta^2} \tag{57}$$

The standard deviation of $|x(t)|/t$ is $\sqrt{\langle |x(t)|^2\rangle - \langle |x(t)|\rangle^2}/t$, and plotting this as a function of β gives a unimodal function with a maximum at some intermediate value of β (or equivalently, noise intensity), as seen in Figure B.6 (bottom). Note that we never calculate the mean of $x(t)$, which we know to be zero from the symmetry of the problem.

Another way to calculate the second moment is to note that the autocorrelation of $I(t)$ is [13,16,36]

$$\langle I(s)I(r)\rangle = v^2 e^{-\beta|s-r|} \tag{58}$$

so that

$$\langle x^2(t)\rangle = \left\langle \int_0^t I(s)\,ds \int_0^t I(r)\,dr \right\rangle = \int_0^t \int_0^t \langle I(s)I(r)\rangle\,ds\,dr = \frac{2v^2(\beta t - 1 + e^{-\beta t})}{\beta^2} \tag{59}$$

Alternatively [32], by multiplying (49) by x^2 and then integrating over x, one obtains the differential equation satisfied by the second moment

$$\frac{d^2\langle x^2\rangle}{dt^2} + \beta\frac{d\langle x^2\rangle}{dt} = 2v^2 \tag{60}$$

The appropriate initial conditions are $\langle x^2\rangle(0) = 0$, $d\langle x^2\rangle/dt|_{t=0} = 0$, and with these, (60) has the solution (59).

Figure B.13 shows the absolute value of the average speed, (51), and one standard deviation from this (using (59)), as a function of noise level. To match Figure B.9, we choose $v = \sqrt{0.2}$ and $t = 1000$. We again use an Arrhenius–type rate to connect switching rate to noise level, fitting the expression $\beta = \Phi e^{-q/D}$ to the data points in Figure B.9 (a least squares fit gives $\Phi = 0.0895, q = 0.0063$).

6 Summary

Spike frequency adaptation can destabilize bumps in networks of spiking neurons and network rate models, leading to traveling bumps [14]. We have shown that adding noise to either a spiking model or a rate model that includes adaptation significantly reduces the average speed of a traveling bump, "restabilizing" it and effectively negating the effect of adaptation. This restabilization occurs for noise levels smaller than those needed to break up the bump. To understand this process we studied a rate model that can be reduced to six ordinary differential equations. From these six equations we constructed a single scalar equation whose non–zero roots are the velocity of the bump and showed that these roots appear in a symmetric pair as the strength of the adaptation is increased. Thus the transition from stationary to moving bump is through a supercritical pitchfork bifurcation in bump speed.

Adding noise to the normal form of a supercritical pitchfork bifurcation, where the variable undergoing the bifurcation is speed, reproduces the observed drop in the absolute value of the average speed as the noise level is increased. The reason for this drop is that noise can change the sign of the speed a number of times during the course of a simulation. Net distance traveled is the integral of speed, so these sign changes result in a decrease in the overall distance traveled, and thus the average speed. The behavior of the full spiking network can therefore be understood in terms

of this noisy normal form. (Bump destabilization is also seen if synaptic depression — another important feature of single neurons — is included, rather than spike frequency adaptation, and adding noise to the depression dynamics can restabilize the bump.)

As a further simplification, we modeled the noisy pitchfork bifurcation as a persistent random walk, in which a particle moves at a constant speed, but the probability of changing direction is constant (and related to noise level through an Arrhenius–type rate). If this process is taken to be continuous in time, the probability density function for position obeys the telegrapher's equation, which has an explicit solution. From this solution we can explicitly construct the mean and standard deviation of the absolute value of the average speed of the particle (quantities that are easily measured from simulations of a full network, the particle being the bump in this case) and they agree quantitatively with the behavior of the full network model.

One aspect of the behavior of a spatially–extended system is not well captured by a persistent random walk: for high noise levels, the position of the maximum of a bump does not necessarily move continuously. The form of the coupling, (3), promotes local activity while suppressing more distant activity, and at high noise levels there can be ongoing "competition" between bumps in a form of "winner takes all" contest. Since the domain is spatially extended, a bump may appear some distance from one that is in the process of disappearing, leading to an effective "jump" in the position of the currently highest bump. (This type of behavior was also seen in [14], in response to a suddenly–moved stimulus.) For both the noisy normal form (33) and the persistent random walks in Section 5, the particle is assumed to move continuously, so this type of jumping will not be captured by these simplified models.

"Restabilization by noise" of a spatiotemporal pattern does not seem to have been discussed elsewhere, although several papers [8,20] contain results regarding the effects of noise strength (manipulated indirectly by changing the number of Brownian walkers in a simulation) on moving "spots" in simulations of excitable media. Our results are an example in the same spirit as stochastic resonance, in which moderate amounts of noise act in a beneficial way (at least in the context of working memory, where a moving bump would be seen to have a detrimental effect on the task). It is not clear which aspects of these systems that support bumps (spatially–extended coupling, a slow variable, traveling structures that appear through a pitchfork bifurcation in speed) are necessary for this restabilization, and the question of which other systems [6,33] show such behavior is an interesting and open one. Figure B.4 shows a counter–example of noise–induced restabilization, where noise causes a traveling wave to break up, rather than slow down.

We have also studied both integrate–and–fire and rate models incorporating synaptic depression [1] rather than, or in addition to, spike frequency adaptation, and such networks also show destabilization of stationary bumps as the strength of the depression is increased and restabilization when noise is added to the dynamics of the depression. This will be reported elsewhere [24]. Models of two–species reaction–diffusion systems

with global coupling [18,21] have been observed to support stationary "spots" and "standing pulses", which begin to move as a parameter is varied, and a similar phenomenon has been seen in both a model three–component reaction–diffusion system in which the only coupling is by diffusion [35], and a pair of coupled Ginzburg–Landau equations [40]. The effects of noise on such systems remains to be investigated.

Acknowledgements

We thank Brent Doiron for a critical reading of the manuscript. This work was supported by NSERC and a PREA award from the government of Ontario.

A Solution of the telegrapher's equation

Since the derivation of the solution of this equation in [32] is incorrect, and that in [15] has a number of typographical errors, we rederive the solution here, following [15]. The telegrapher's equation is

$$\frac{\partial^2 p}{\partial t^2} + \beta \frac{\partial p}{\partial t} = v^2 \frac{\partial^2 p}{\partial x^2} \tag{A.1}$$

with initial conditions $p(x,0) = \delta(x)$ and $\partial p(x,t)/\partial t|_{t=0} = 0$. The Fourier transform of p is

$$\sigma(s,t) = \int_{-\infty}^{\infty} p(x,t) e^{-isx}\, dx \tag{A.2}$$

which satisfies

$$\frac{d^2\sigma}{dt^2} + \beta \frac{d\sigma}{dt} + v^2 s^2 \sigma = 0 \tag{A.3}$$

with initial conditions $\sigma(s,0) = 1$ and $d\sigma(s,t)/dt|_{t=0} = 0$. The solution of (A.3) with these initial conditions is

$$\begin{aligned}\sigma(s,t) &= e^{-\beta t/2} \left[\cos\left(t\sqrt{v^2 s^2 - \beta^2/4} \right) \right. \\ &\quad \left. + \frac{\beta}{2\sqrt{v^2 s^2 - \beta^2/4}} \sin\left(t\sqrt{v^2 s^2 - \beta^2/4} \right) \right] \qquad \text{(A.4)} \\ &= e^{-\beta t/2} \left(\frac{\beta}{2} + \frac{\partial}{\partial t} \right) \left\{ \frac{1}{\sqrt{v^2 s^2 - \beta^2/4}} \sin\left(t\sqrt{v^2 s^2 - \beta^2/4} \right) \right\} \qquad \text{(A.5)}\end{aligned}$$

Since p is real, the inverse Fourier transform of (A.5) is

$$p(x,t) = \frac{e^{-\beta t/2}}{2\pi}\left(\frac{\beta}{2}+\frac{\partial}{\partial t}\right)\int_{-\infty}^{\infty}\frac{\cos(sx)}{\sqrt{v^2s^2-\beta^2/4}}\sin\left(t\sqrt{v^2s^2-\beta^2/4}\right)ds \tag{A.6}$$

$$= \frac{e^{-\beta t/2}}{2v}\left(\frac{\beta}{2}+\frac{\partial}{\partial t}\right)\left\{H(vt-|x|)I_0\left(\frac{\beta}{2v}\sqrt{v^2t^2-x^2}\right)\right\} \tag{A.7}$$

and performing the differentiation gives (50).

References

[1] L. F. Abbott, J. A. Varela, K. Sen and S. B. Nelson. Synaptic depression and cortical gain control. Science. **275** (1997), 220-223.

[2] S. Amari. Dynamics of pattern formation in lateral–inhibition type neural fields. Biol. Cybern. **27** (1977), 77-87.

[3] R. Ben–Yishai, R. L. Bar–Or and H. Sompolinsky. Theory of orientation tuning in visual cortex. Proc. Natl. Acad. Sci. USA. **92**, (1995) 3844-3848.

[4] P. C. Bressloff, N. W. Bressloff and J. D. Cowan. Dynamical mechanism for sharp orientation tuning in an integrate–and–fire model of a cortical hypercolumn. Neural Comp. **12** (2000), 2473-2511.

[5] A. Compte, N. Brunel, P. S. Goldman–Rakic and X.–J. Wang. Synaptic mechanisms and network dynamics underlying spatial working memory in a cortical network model. Cereb. Cortex **10** (2000), 910-923.

[6] G. B. Ermentrout. Neural networks as spatio–temporal pattern–forming systems. Rep. Prog. Phys. **61** (1998), 353-430.

[7] R. F. Fox, I. R. Gatland, R. Roy and G. Vemuri. Fast, accurate algorithm for numerical simulation of exponentially correlated colored noise. Phys. Rev. A **38** (11) (1988), 5938-5940.

[8] T. Fricke and L. Schimansky–Geier. Moving spots in three dimensions. In Activator–Inhibitor Dynamics. Ed. H. Engel et al. Verlag Technik Berlin (1996). 184.

[9] L. Gammaitoni, P. Hänggi, P. Jung and F. Marchesoni. Stochastic resonance. Rev. Mod. Phys. **70**(1) (1998), 223-287.

[10] C. W. Gardiner. Handbook of stochastic methods for physics, chemistry and the natural sciences. Berlin, New York, Springer–Verlag. 1983.

[11] J. Guckenheimer and P. Holmes. Nonlinear oscillations, dynamical systems and bifurcations of vector fields. Applied Mathematical Sciences, Vol. 42. Springer–Verlag. 1990.

[12] B. S. Gutkin, C. R. Laing, C. L. Colby, C. C. Chow and G. B. Ermentrout. Turning on and off with excitation: the role of spike–timing asynchrony and synchrony in sustained neural activity. J. Comp. Neurosci. **11**(2) (2001).

[13] P. Hänggi and P. Riseborough. Activation rates in bistable systems in the presence of correlated noise. Phys. Rev. A **27**, (1983). 3379-3382.

[14] D. Hansel and H. Sompolinsky. Modeling feature selectivity in local cortical circuits. In Methods in Neuronal Modeling: From Ions to Networks. Ed. C. Koch and I. Segev. MIT Press (1998). 499-567.

[15] P. Chr. Hemmer. On a generalization of Smoluchowski's diffusion equation. Physica **27** (1961), 79-82.

[16] W. Horsthemke and R. Lefever. Noise–induced Transitions. Series in Synergetics, Vol. 15. Springer–Verlag, 1984.

[17] P. Jung, A. Cornell–Bell, F. Moss, S. Kadar, J. Wang and K. Showalter. Noise sustained waves in subexcitable media: From chemical waves to brain waves. Chaos **8**(3) (1998), 567-575.

[18] S. Kawaguchi and M. Mimura. Collision of travelling waves in a reaction diffusion system with global coupling effect. SIAM J. Appl. Math. **59**(3), (1999), 920-941.

[19] E. Knobloch and K. A. Wiesenfeld. Bifurcations in fluctuating systems: the center–manifold approach. J. Stat. Phys. **33**(3), (1983), 611-637.

[20] M. Kostur and L. Schimansky–Geier. Simulations of localized dissipative structures in excitable media by an ensemble of Brownian walkers. Acta Phys. Polon. B **32**(2), (2001), 351-360.

[21] K. Krischer and A. Mikhailov. Bifurcation to traveling spots in reaction–diffusion systems. Phys. Rev. Lett. **73**(23), (1994), 3165-3168.

[22] C. R. Laing and C. C. Chow. Stationary bumps in networks of spiking neurons. Neural Comp. **13** (7), (2001), 1473-1494.

[23] C. R. Laing and A. Longtin. Stabilization of spatiotemporal patterns by noise. Submitted to Phys. Rev. Lett. (2001).

[24] C. R. Laing and A. Longtin. In preparation, 2001.

[25] C. R. Laing, A. McRobie and J. M. T. Thompson, The post–processed Galerkin method applied to non–linear shell vibrations. Dyn. Stab. Systems **14** (1999), 163-181.

[26] Y.-H. Liu and X.-J. Wang. Spike–frequency adaptation of a generalized leaky integrate–and–fire model neuron. J. Comp. Neurosci. **10** (2001), 25-45.

[27] M. Löcher, N. Chatterjee, F. Marchesoni, W. L. Ditto and E. R. Hunt. Noise sustained propagation: local versus global noise. Phys. Rev. E. **61**(5), (2000), 4954-4961.

[28] A. Longtin. Noise–induced transitions at a Hopf bifurcation in a first–order delay–differential equation. Phys. Rev. A **44**(8) (1991), 4801-4813.

[29] A. Manwani and C. Koch. Detecting and estimating signals in noisy cable structures, I: neuronal noise sources. Neural Comp. **11**(8) 1999, 1797-1829.

[30] J. Masoliver, K. Lindenberg and B. J. West. First–passage times for non–Markovian processes. Phys. Rev. A **33**, (1986), 2177-2180.

[31] J. Masoliver, K. Lindenberg and B. J. West. First–passage times for non–Markovian processes: Correlated impacts on a free process. Phys. Rev. A **34**, (1986), 1481-1494.

[32] J. Masilover and G. H. Weiss. Finite–velocity diffusion. Eur. J. Phys. **17**, (1996), 190-196.

[33] J. Murray. Mathematical Biology. Biomathematics, Vol. 19. Springer–Verlag. 1993.

[34] F.-J. Niedernostheide, B. S. Kerner and H.-G. Purwins. Spontaneous appearances of rocking localized current filaments in a nonequilibrium distributive system. Phys. Rev. B. **46**(12), (1992), 7559-7570.

[35] M. Or-Guil, M. Bode, C. P. Schenk and H.-G. Purwins. Spot bifurcations in three–component reaction–diffusion systems: The onset of propagation. Phys. Rev. E. **57**(6), (1998), 6432-6437.

[36] A. Papoulis. Probability, random variables, and stochastic processes. Third edition. McGraw–Hill, 1991.

[37] V. Pérez-Muñuzuri, F. Sagés and J. M. Sancho. Lifetime enhancement of scroll rings by spatiotemporal fluctuations. Phys. Rev. E. **62**(1), (2000), 94-99.

[38] A. D. Redish, A. N. Elga and D. S. Touretzky. A coupled attractor model of the rodent head direction system. Network. **7**(4), (1996) 671-685.

[39] J. Rubin, D. Terman and C. Chow. Localized bumps of activity sustained by inhibition in a two–layer thalamic network. J. Comp. Neurosci. **10**(3), (2001) 313-331.

[40] H. Sakaguchi and B. A. Malomed. Instabilities and splitting of pulses in coupled Ginzburg–Landau equations. Physica D. **154** (2001), 229-239.

[41] J. M. Sancho. Stochastic processes driven by dichotomous Markov noise: some exact dynamical results. J. Math. Phys. **25**(2) (1984), 354-359.

[42] M. Schumaker. Center manifold reduction and normal form transformations in systems with additive noise. Phys. Lett. A. **122** (1987), 317-322.

[43] J. Sneyd and J. Sherratt. On the propagation of calcium waves in an inhomogeneous medium. SIAM J. Appl. Math. **57**(1), (1997) 73-94.

[44] X.-J. Wang. Synaptic reverberation underlying mnemonic persistent activity. Trends Neurosci. **24**(8), (2001) 455-463.

[45] K. Wiesenfeld and F. Jaramillo. Minireview of stochastic resonance. Chaos **8**(3) (1998), 539-548.

B Figures

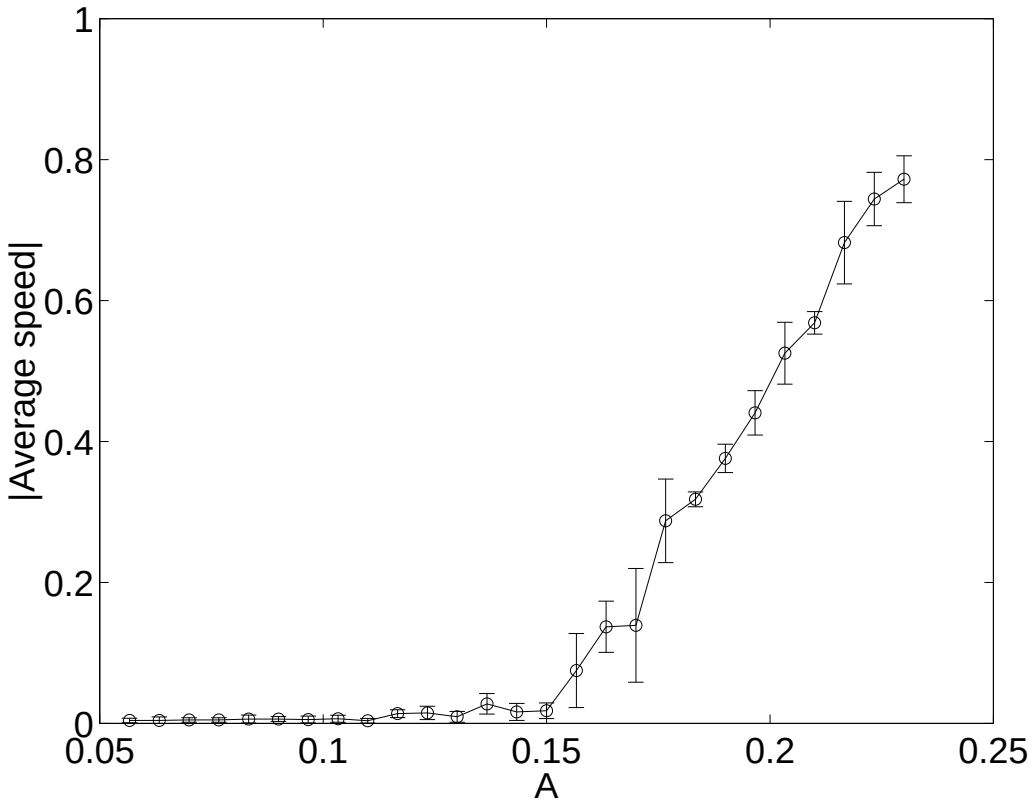

Fig. B.1. Absolute value of the speed of a bump during a period of 480 time units for the spiking neuron model, equations (1)-(2) as a function of A. Error bars are $\pm$ one standard deviation from the mean. Different initial conditions lead to slightly different values of speed, as (1)-(2) is a highly nonlinear and high–dimensional, possibly chaotic, deterministic dynamical system (For example, note the fluctuations about the smooth motion in Figure B.2, left panel).

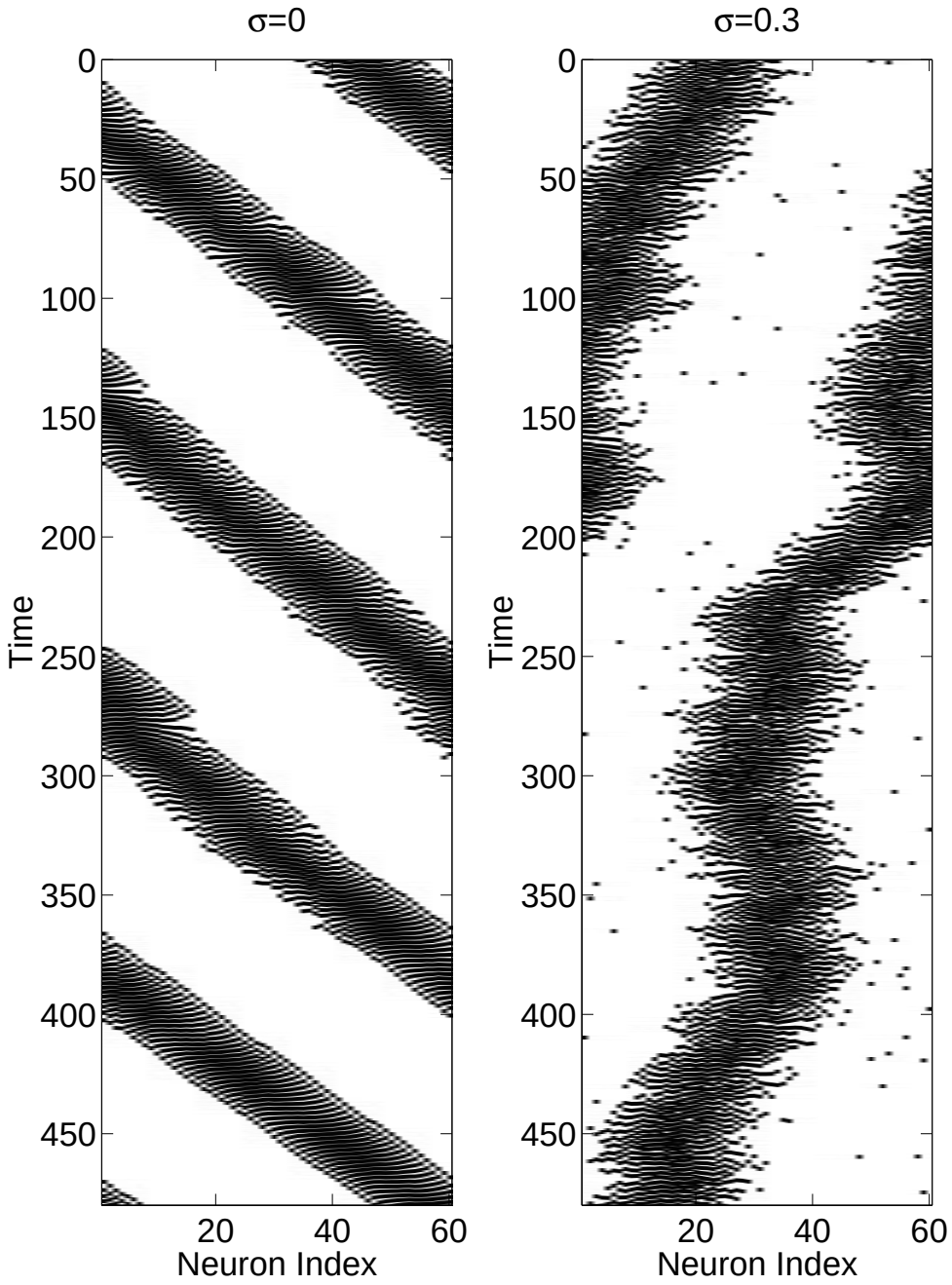

Fig. B.2. Rastergrams of the activity in the integrate–and–fire network (1)-(2). Left panel: $\sigma = 0$ (i.e. no noise), right panel: $\sigma = 0.3$. $A = 0.2$ for both. A "dot" represents the firing of an individual neuron. The sloped bands represent moving localized bumps of activity (recall that the boundary conditions are periodic). The fluctuations in bump size and shape in the left panel are of deterministic origin — see text for discussion.

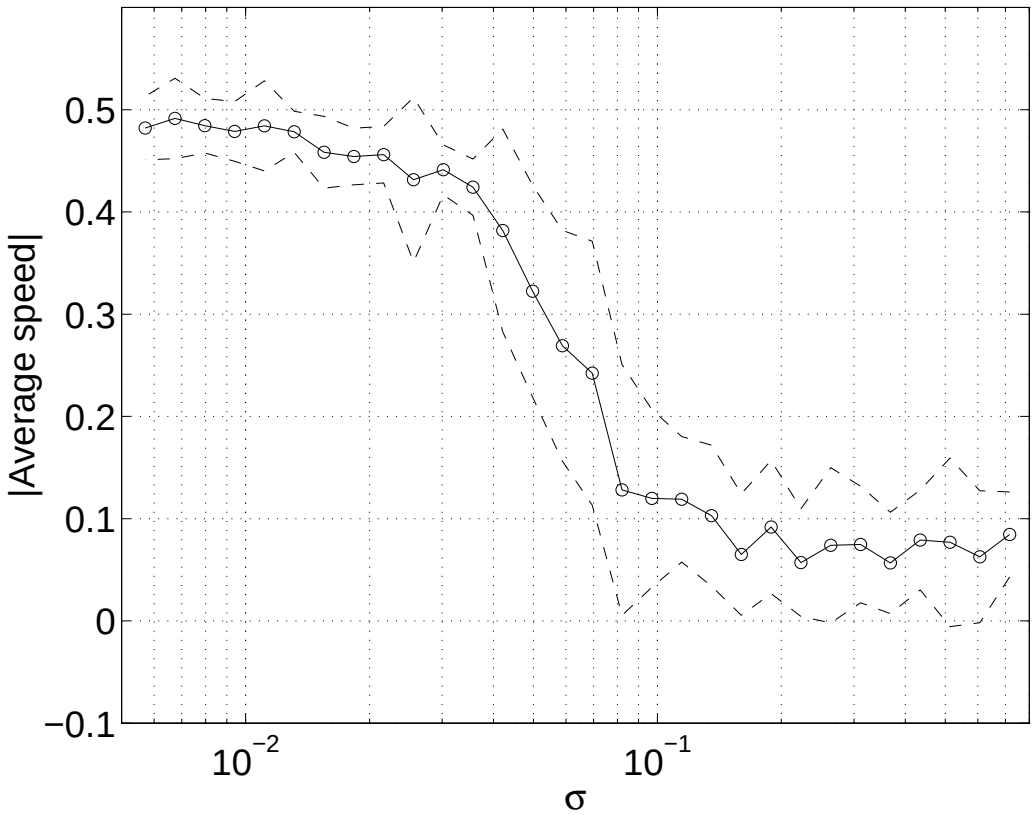

Fig. B.3. Absolute value of the average speed of a bump during a period of 480 time units as a function of noise level, for the spiking neuron model, equations (1)-(2). Parameter values are given in the text. Dashed lines are ± one standard deviation from the mean. We have set $A = 0.2$.

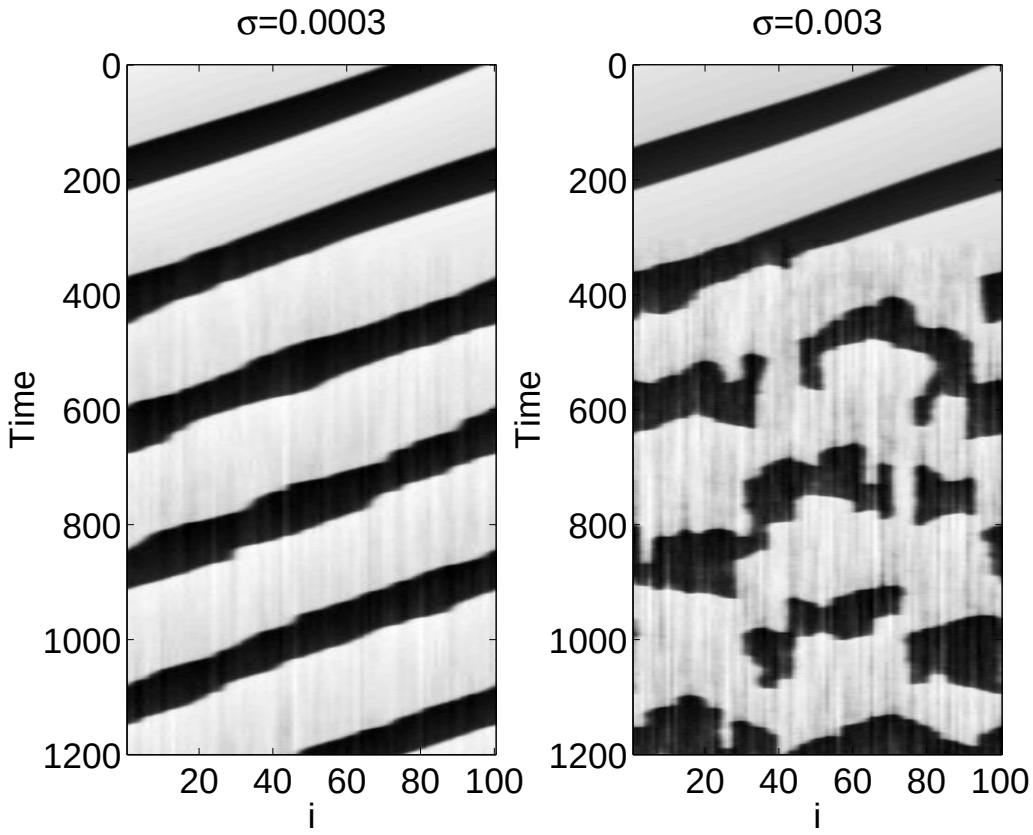

Fig. B.4. The effects of Gaussian white noise on a traveling wave solution in a one–dimensional ring of Fitzhugh–Nagumo excitable cells, (4)-(5). Noise with intensity σ is introduced at $t = 300$. Boundary conditions are periodic, and parameters are $D = 1$, $\delta x = 1$, $\epsilon = 0.005$, $\gamma = 0.5$ and $b = 0.6$. u is plotted, with black representing high values and white, low values.

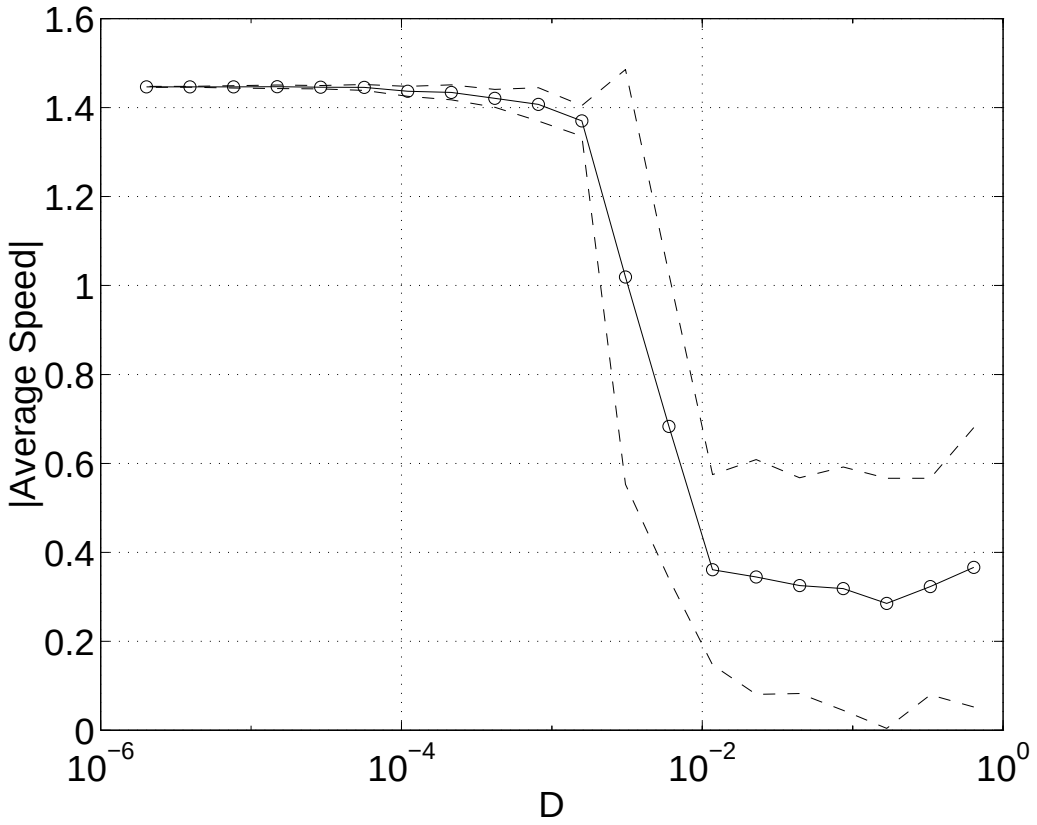

Fig. B.5. Absolute value of the average speed of a bump during a period of 750 time units as a function of noise level, for the spatially–discretized rate model, (8) and (10). Parameter values are given in the text. Dashed lines are ± one standard deviation from the mean.

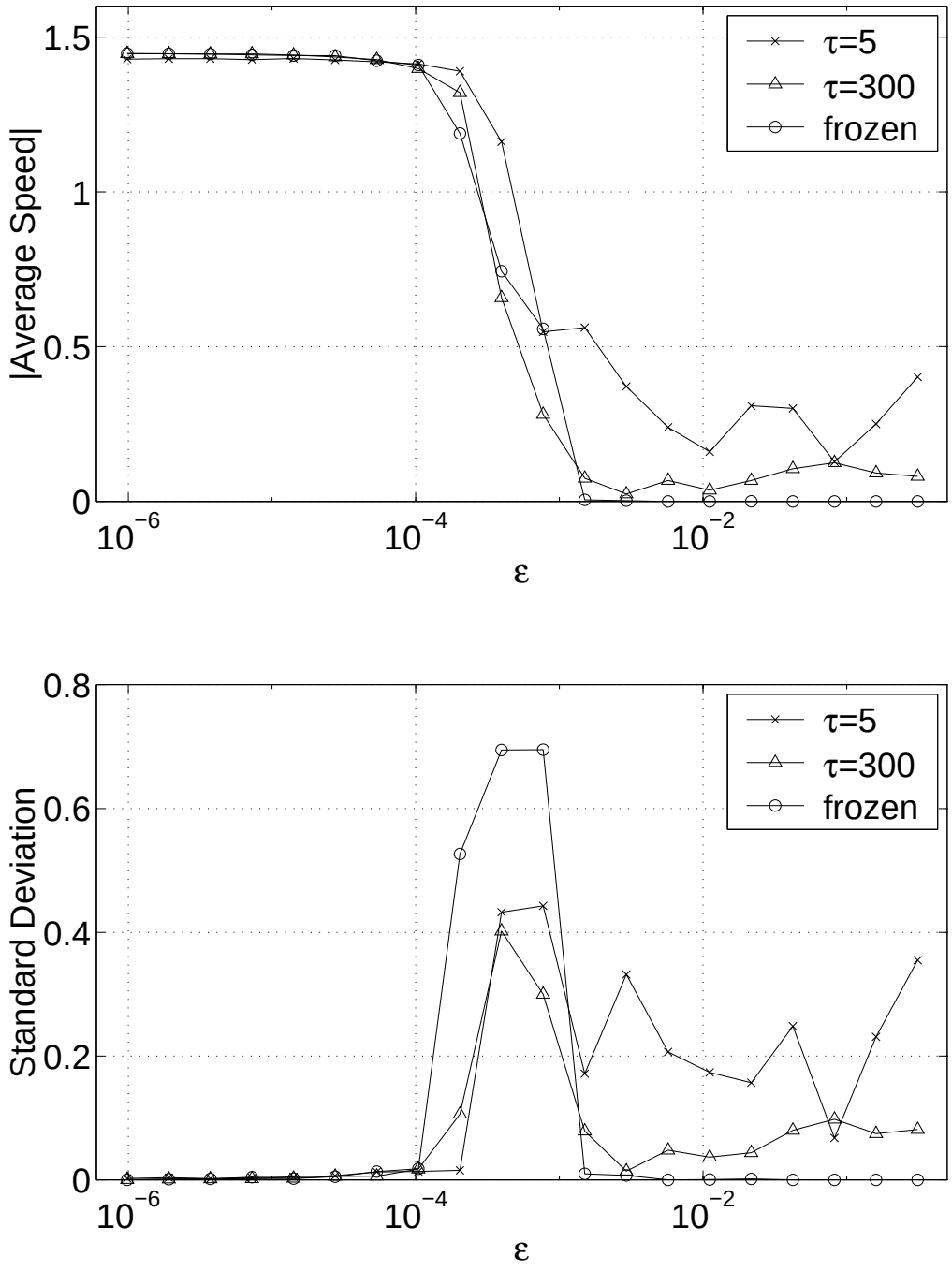

Fig. B.6. Top: Absolute value of the average speed of a bump during a period of 750 time units as a function of colored noise level or "power", ε, for the spatially-discretized rate model, (8) and (11). Bottom: Standard deviation of the absolute value of the average speed. The standard deviation is zero only for strong enough frozen noise. See text for details of the noise.

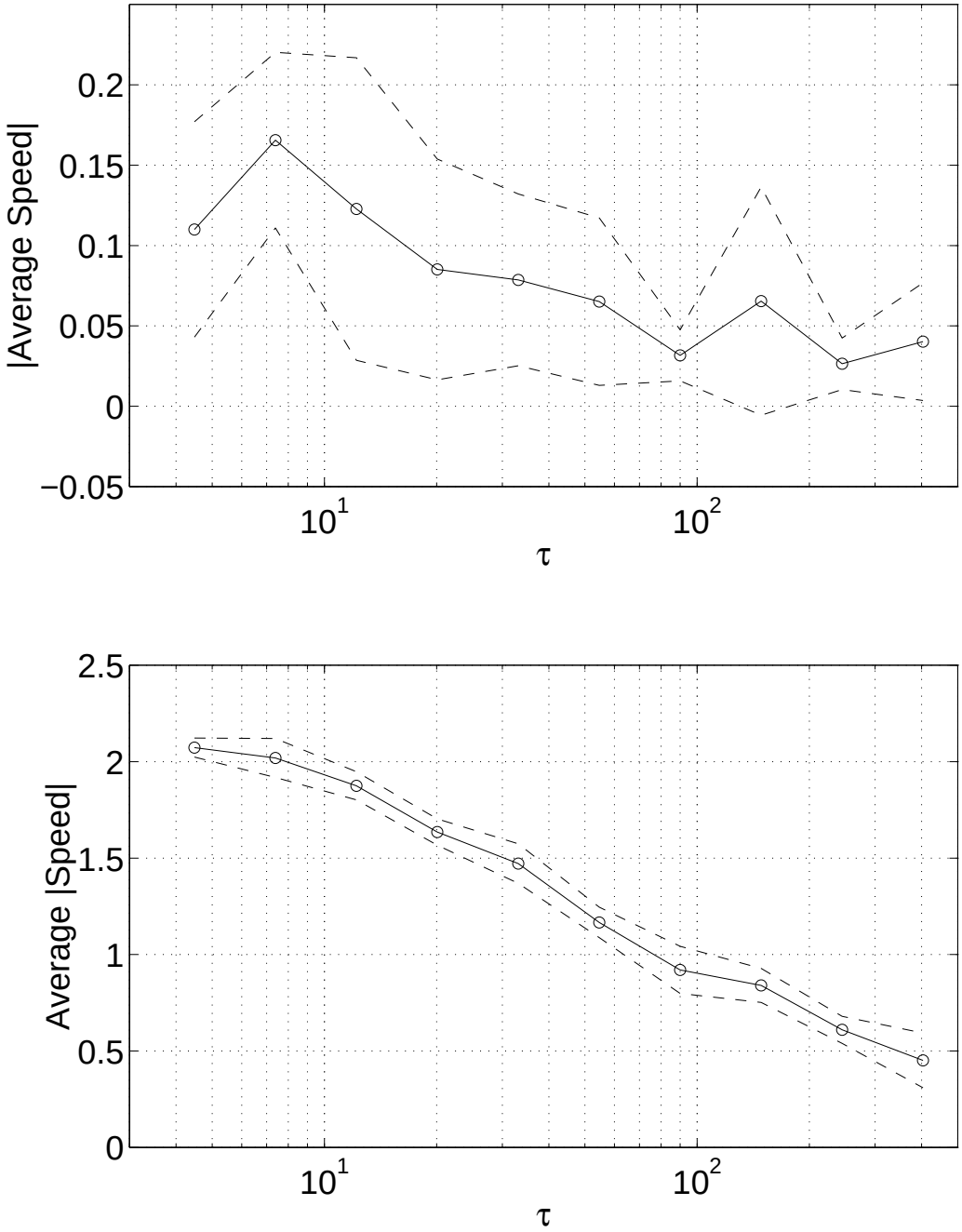

Fig. B.7. Top: Absolute value of the average speed of a bump during a period of 2400 time units as a function of noise correlation time, τ, for equations (8) and (11). Noise power $\varepsilon = 0.1$. Bottom: Average of the absolute value of the instantaneous speed. Dashed lines indicate $\pm$ one standard deviation.

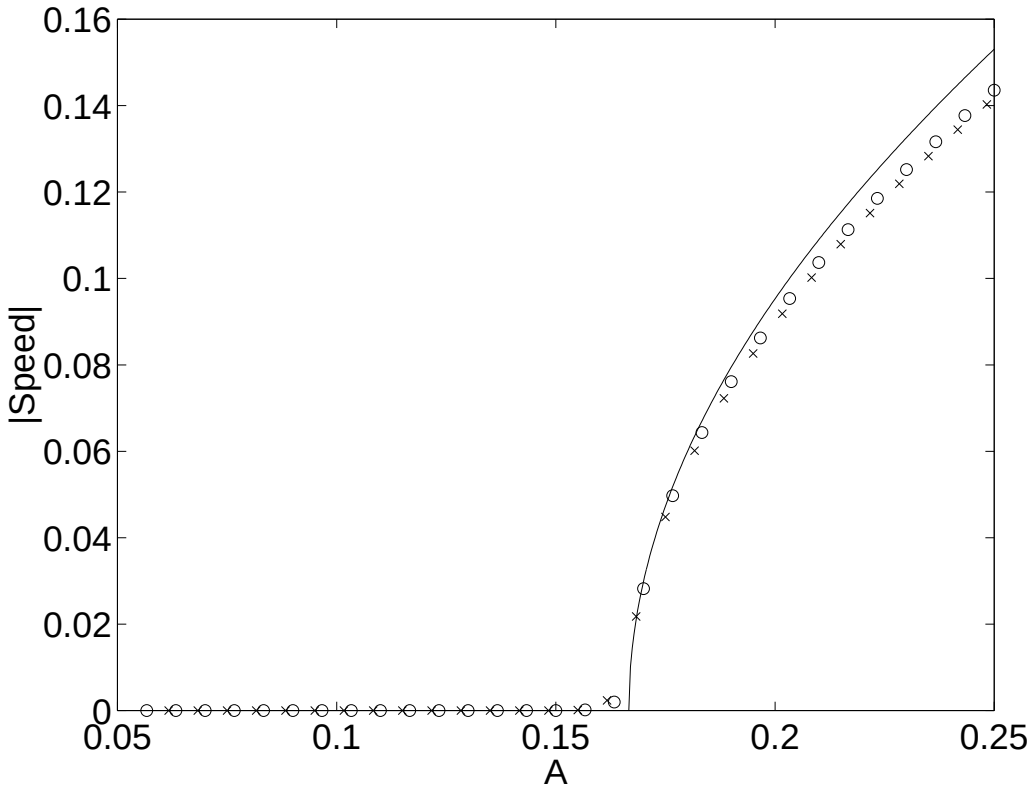

Fig. B.8. Absolute value of the speed of a bump for the rate model (8)-(9) ("o"), equations (14)-(19) ("x", using the same parameters as in (8)-(9)), and the expression (32) (solid line).

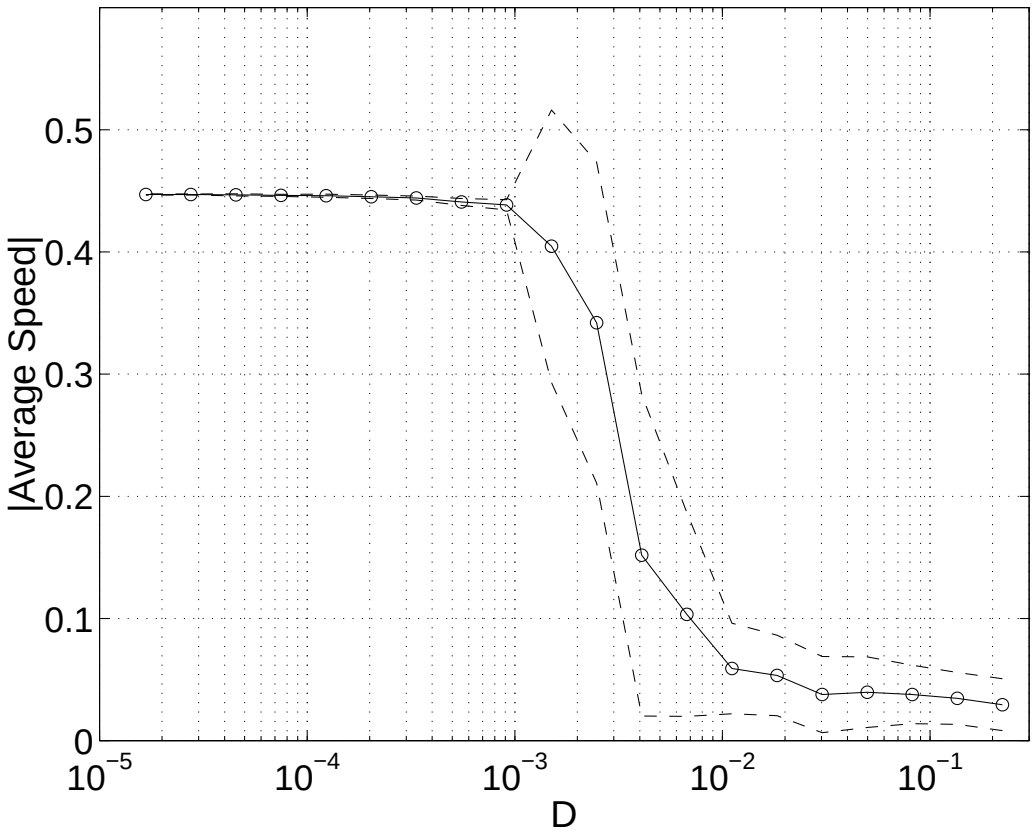

Fig. B.9. Absolute value of average rate of change of θ for the normal form of a supercritical pitchfork bifurcation (33) during 1000 time units, i.e. $|\theta(1000) - \theta(0)|/1000$, as a function of noise intensity, D. $\lambda = 0.2$. The variability is a result of taking multiple noise realizations. The dashed lines indicate $\pm$ one standard deviation. Compare with Figures B.3 and B.5.

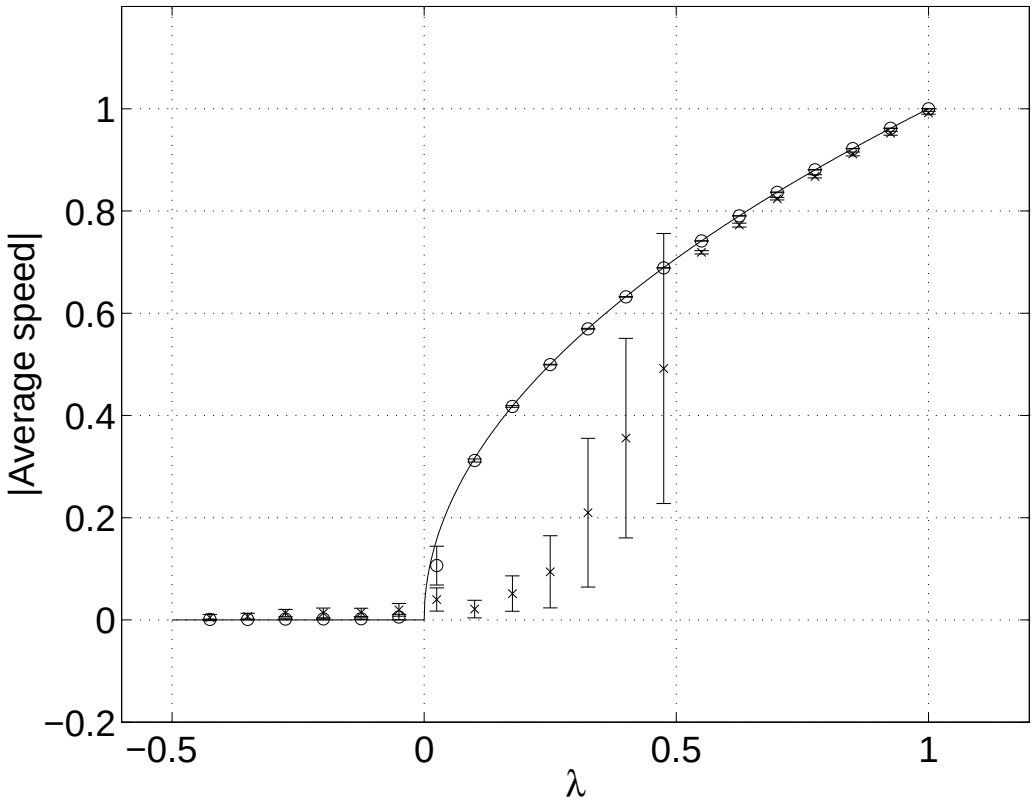

Fig. B.10. Absolute value of average rate of change of θ for the normal form of a supercritical pitchfork bifurcation (33) during 1000 time units as a function of λ. "o": $D = 10^{-4}$, "x": $D = 10^{-2}$. Solid line: $\sqrt{\lambda}$ for $\lambda > 0$, 0 otherwise. Errorbars indicate $\pm$ one standard deviation.

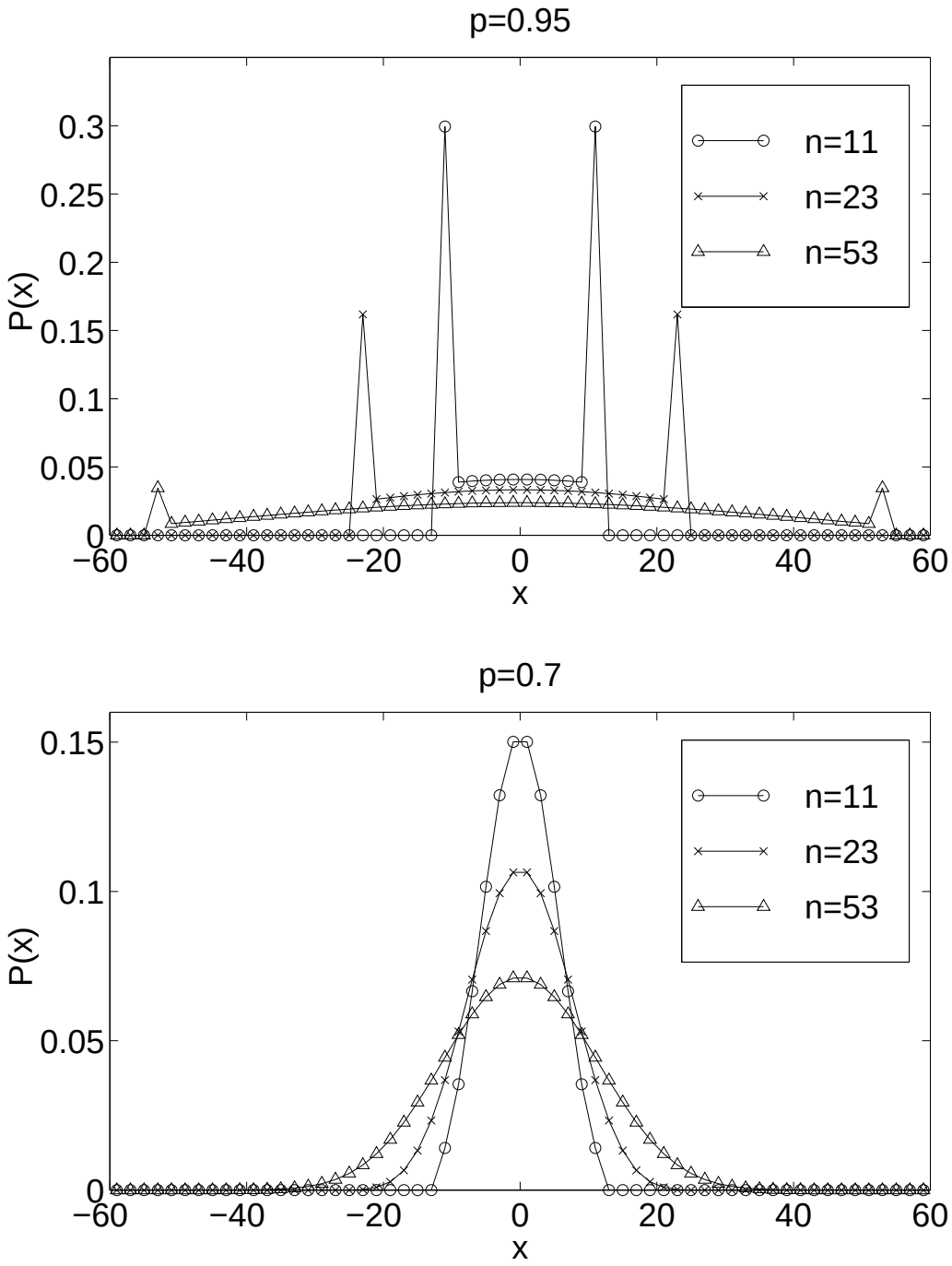

Fig. B.11. $P(x)$ for the discrete–time persistent random walk on a lattice, as calculated using (39)-(46) at different values of x for $p = 0.95$ (top) and $p = 0.7$ (bottom). Only odd values of x are used, as $P(x) = 0$ for even x.

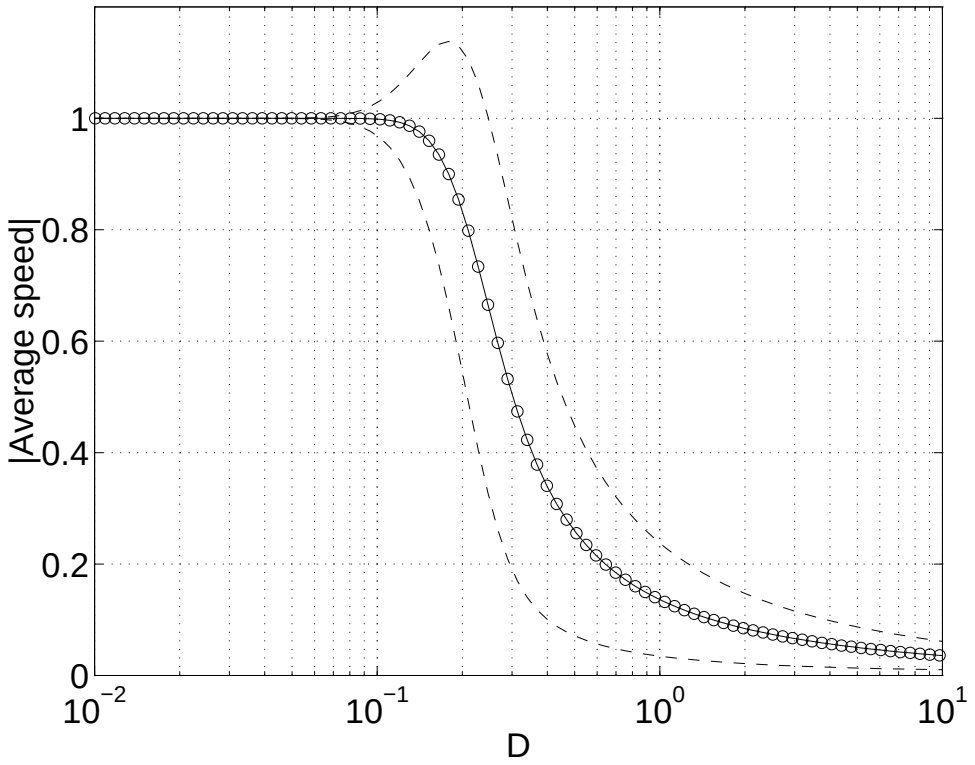

Fig. B.12. Absolute value of average speed for the discrete–time persistent random walk during 59 steps. The probability of traveling in the same direction, p, is given by $p = 1 - e^{-1/D}$. The dashed lines indicate $\pm$ one standard deviation. Compare with Figures B.3, B.5 and B.9.

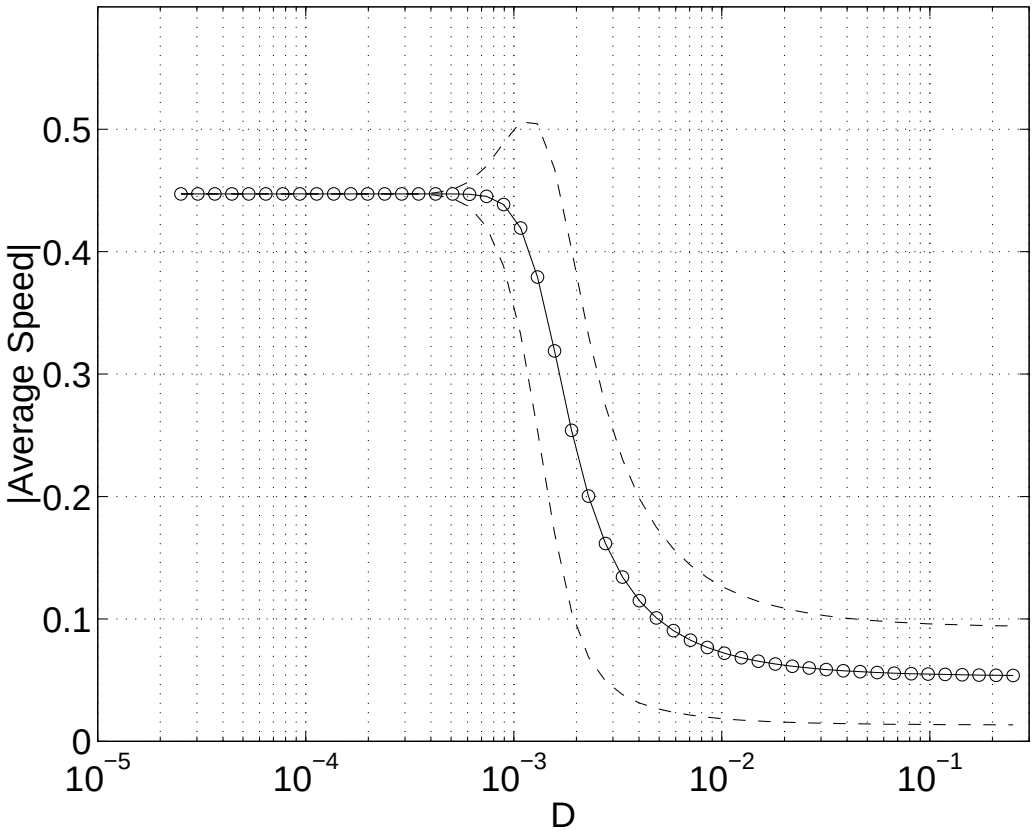

Fig. B.13. Absolute value of average speed, (51), as a function of noise intensity for the continuous persistent random walk. In order to match Figure B.9 we set $v = \sqrt{0.2}$, $t = 1000$, and a least squares fit to the data in Figure B.9 gives $\beta = 0.0895e^{-0.0063/D}$. The dashed lines indicate $\pm$ one standard deviation, from (59). Compare with Figures B.9 and B.12.

C Tables

Path	Probability	Distance
000	$p^2/2$	3
001	$p(1-p)/2$	1
010	$(1-p)^2/2$	1
011	$p(1-p)/2$	-1
100	$p(1-p)/2$	1
101	$(1-p)^2/2$	-1
110	$p(1-p)/2$	-1
111	$p^2/2$	-3

Table C.1
Possible paths, probability of taking paths, and distance moved, for three steps of a discrete–time persistent random walk.